

---

# A survey of parametric modelling methods in high-speed train head design

Ruibin Wang<sup>1</sup>, Jianjun Zhang<sup>1,2</sup>, Shaojun Bian<sup>2</sup> and Lihuan You<sup>2</sup>

<sup>1</sup>State Key Laboratory of Traction Power, Southwest Jiaotong University, Chengdu, China

<sup>2</sup>National Centre for Computer Animation, Bournemouth University, Poole, UK

Corresponding author: Jian J. Zhang, jzhang@bournemouth.ac.uk

## Abstract

With the continuous increase of the running speed, the head shape of the high-speed train (HST) turns out to be a critical factor for further speed boost. In order to cut down the time used in the HST head design and improve the modelling efficiency, various parametric modelling methods have been widely applied in the optimization design of the HST head to obtain an optimal head shape so that the aerodynamic effect acting on the head of HSTs can be reduced and more energy can be saved. This paper reviews these parametric modelling methods and classifies them into four categories: 2D, 3D, CATIA-based, and mesh deformation-based parametric modelling methods. Each of the methods is introduced, and the advantages and disadvantages of these methods are identified. The simulation results are presented to demonstrate that the aerodynamic performance of the optimal models constructed by these parametric modelling methods has been improved when compared with numerical calculation results of the original models or the prototype models of running trains. Since different parametric modelling methods used different original models and optimization methods, few publications could be found which compare the simulation results of the aerodynamic performance among different parametric modelling methods. In spite of this, these parametric modelling methods indicate more local shape details will lead to more accurate simulation results, and fewer design variables will result in higher computational efficiency. Therefore, the ability of describing more local shape details with fewer design variables could serve as a main specification to assess the performance of various parametric modelling methods. The future research directions may concentrate on how to improve such ability.

## Keywords

Parametric methods, head design, high-speed trains, 2D contour representations in side view, profile definitions for 3D shapes, CATIA-based parameterization, mesh deformation-based modelling

## Introduction

In recent years, HSTs have got an increasing development around the world, which makes the normal transportation more diversified and convenient. With the increasing speed of HSTs, some aerodynamic effects ignored at a low speed such as the aerodynamic drag, the pressure wave, and the micro-pressure wave have limited the further increment of the HST speed<sup>1</sup>. The head shape plays an important role in improving these aerodynamic effects.

The aerodynamic drag affects the improvement of the running speed. The head shape of HSTs has a large influence on the aerodynamic drag. As Tian et al. pointed out, at a speed of 300 km/h, the aerodynamic drag takes 85% of the total resistance when the length of the streamlined heads is larger than 5 m, and reduces to 75% when the length of the train heads is out of 10 m which leads to a conclusion that a reasonable head shape of HSTs can improve its aerodynamic performance obviously<sup>2</sup>. Iida et al.<sup>8</sup> stated that the air ahead of the train nose is compressed as a train enters a tunnel, and another pressure wave is generated as the train nose leaves the tunnel. Micro-pressure wave is mainly affected by train speed, train-to-tunnel area ratio, slenderness ratio, slenderness and shape of train nose, etc. Lee and Kim<sup>13</sup> designed the three-dimensional nose shape to minimize the maximum micro-pressure wave.

At present, there are mainly four countries that can construct the HSTs with a design speed higher than 300 km/h. As shown in Fig. 1, these HSTs are ICE3 series, Shinkansen series (E7), CRH380 series and TVG series. Each series not only focuses on improving its aerodynamic performance but also takes its running conditions into consideration. In order to reduce the

aerodynamic drag and the micro pressure wave when HSTs enter a tunnel, the head shape of Shinkansen series is designed with a large slenderness ratio. ICE3 series and TGV series mainly focus on reducing aerodynamic drag and aerodynamic lift of HSTs. CRH380 series is designed based on Shinkansen E2 series, which fully considers its domestic operating environments and aerodynamic performance.

The head shape of the HST is a complex streamlined type with dozens of design variables which makes the design process more difficult. Generally, the design of HSTs involves wind tunnel tests, numerical simulations and real vehicle tests to obtain an optimal train head shape. Such a design process is expensive, time-consuming, and not suitable for modern design of HSTs.



Fig. 1 HST with a design speed greater than 300 km/h

Some work has been done to simplify the design process. Maeda et al.<sup>3</sup> gave several reasonable suggestions for reducing the aerodynamic drag for Shinkansen 100 series, 0 series and 200 series. Raghunathan<sup>1</sup> designed 16 sets of simple train head models to study the relationship among the cross-sectional area distribution of the train head, aerodynamic drags and airflow velocities. In order to investigate the influence of the train nose section configuration on the pressure variation, KiKuChi et al.<sup>4</sup> analyzed three types of nose shape (circular-cone type, middle type and wedge type) with different nose length using the three-dimensional boundary element method, while the maximum train cross-sectional area is fixed and the train nose section configuration is changed. Then they figured out that the reduction of the pressure variation is larger if the nose is longer when the nose section configuration is the same and the reduction of the pressure variation of wedge type is larger than that of cone type when the nose section length is the same. By testing several sets of simple train head models, Choi et al.<sup>5</sup> found that the aerodynamic drags reduced up to approximately 50% when the train head is changed from a blunt shape to a streamlined shape. Hemida et al.<sup>6</sup> investigated the impact of the head length on the dynamic performance and the fluid structure of the HST by simulating the short nose model at the 90° yaw angle repeatedly. The results indicated that the HST with a short head was highly unsteady. Essentially, all these methods need to generate the shape of HST heads before the simulation, which heavily relies on the existing experience. Moreover, the obtained model is not the optimal one.

In order to tackle the above problems, the general method is to create a parametric model, and use computer software to adjust design variables automatically in the optimization process. Then a model with the optimal aerodynamic performance is obtained with some optimized methods such as genetic algorithm, surrogate model and multi-objective optimization algorithm, etc. These optimization methods have a common feature: the more design variables are involved, the more time is required in the process of optimization. In order to improve the efficiency, it is necessary to reduce the number of design variables. But this will make some detailed parts of the train head cannot be described. Therefore, it is very important to use less variables to control the shape of the train head accurately. Various modelling methods have been proposed to address this issue.

The 2D modelling methods are mainly focus on the longitudinal distribution of the cross-sectional area, because the main factors such as the length, the bluntness, the cross-sectional shape and the cross-sectional area of the train head which affect the aerodynamic performance a lot are involved in this part<sup>10</sup>. Some detailed parts (such as the drain, driver cab, cowcatcher etc.) cannot be described though the 2D modelling methods have a big advantage in time consumption. Iida et al.<sup>7,8</sup> put forward a numerical optimization method to design the train head, where two parametric variables were used to consider the longitudinal distribution of the cross-sectional area in control. Kwon et al.<sup>12</sup> adopted the Hick-Henne function to parameterize the head shape of HST which provides more degrees for the designing

process. Several modifications and combinations were made based on those two methods, which was proved more effective<sup>10,13,15,16</sup>. The idealized train model, the 2D elliptic curve model and the Bézier curve model were also designed to study the aerodynamic performance of the high-speed train head<sup>6,17,18,19,20,21</sup>.

In contrast, 3D modelling methods use more factors to improve the modelling accuracy but this means more time is consumed in the process of optimization. Generally, there are three ways to parameterize the head shape in the 3D space. The first way is to parameter the main control lines of the train head, such as the vehicle modelling function (VMF) method<sup>14</sup>, and the combination of B-spline curves and Coons patches<sup>22</sup>. The second way is to control the shape of the train head with some parametric modelling software, such as the CATIA-based three-parameters<sup>23</sup>. The final way is to control the deformation of the grid points on the surfaces of the train head, such as the arbitrary shape deformation (ASD) technique<sup>27,28</sup>.

In this paper, several latest parametric modelling methods on the HST head shape design are summarized. These methods are divided into four categories. The related models and the modelling steps involved in each method are described whilst their advantages and disadvantages are identified. Some potential research directions are discussed finally.

## Methodology

The contour line shape has a big effect on the aerodynamic performance of the train head. Different head shapes are determined by different contour line functions. Therefore, various parametric modelling methods focus on how to choose proper contour line functions to parameterize the head shape.

In this section, we classify various parametric modelling methods into four categories. 2D parametric modelling methods, only defining one contour of HST heads without sufficient information to describe 3D head models, will be first reviewed. 3D parametric modelling methods which provide more contours enough to define 3D head models will be reviewed next. After that, CATIA-based parametric modelling which uses the software package CATIA to create 3D head models from parametric descriptions will be introduced. Finally, three mesh deformation-based parametric modelling methods will be discussed.

### 2D parametric modelling methods

Two-dimensional (2D) parametric modelling methods use few parameters to define one main contour line of the HST heads in a side view. Since they do not provide sufficient information to define 3D train head models, these methods are classified into 2D parametric modelling. In this subsection, the 2D shapes are classified into two types: the 2D axisymmetric shapes and the 2D planar shapes. The longitudinal profile of 2D axisymmetric shapes are mainly controlled by its cross-sectional area distribution. When the cross-sectional area distribution of the HST head is optimized, its 3D shape is also optimized<sup>22</sup>. The 2D planar shapes are mainly controlled by the shape of its longitudinal profiles directly. It is proved that the 2D axisymmetric shapes are more suitable to planar MPW(micro-pressure wave) problems because it has the same longitudinal profiles and the same cross-section along the train length as its corresponding 3D model<sup>11</sup>. The 2D planar shapes are important in reducing aerodynamic drags because its can provide more design variables to obtain the optimum shape. Five 2D parametric modelling models will be reviewed below. The Iida's model and the Hicks-Henne function-based model belong to the 2D axisymmetric shapes; The idealised train model, the 2D elliptic curve model and the Bézier curve model belong to the 2D planar shapes.

*The Iida's model.* In order to optimize the train head shape for reducing the micro pressure wave at the exit of the tunnel, Iida et al.<sup>7,8</sup> proposed a parametric model below controlled by two parametric variables  $\alpha_1$  and  $\alpha_2$  to describe the longitudinal distribution function of the cross-sectional area of the train head

$$\frac{A_T(s)}{\pi b^2} = (1 - \alpha_2) \left[ (1 - \alpha_1) \frac{s}{a} + \alpha_1 \sqrt{\frac{s}{a}} \right] + \alpha_2 \left( \frac{s}{a} \right)^2, \quad (1)$$

where  $s$  is the distance between the nose tip and the points on the contour line,  $a$  is the

length of the train head and  $b$  is the maximum radius of the train head. The two design variables  $\alpha_1$  and  $\alpha_2$  control the shape of the HST head. When  $\alpha_1 = 0$  and  $\alpha_2 = 0$ , the longitudinal distribution of the cross-sectional area is linear and the shape of the train head is a paraboloid of revolution. When  $\alpha_1 = 0$  and  $\alpha_2 = 1$ , the longitudinal distribution of the cross-sectional area is parabolic, and the shape of the train head is a circular cone. Iida et al.<sup>8</sup> figured out the cross-sectional area distribution and radius distribution of optimum nose shape compared with other 2D axisymmetric shapes (the paraboloid shape, the ellipsoid shape and the circular cone shape) which is shown in Fig. 2.

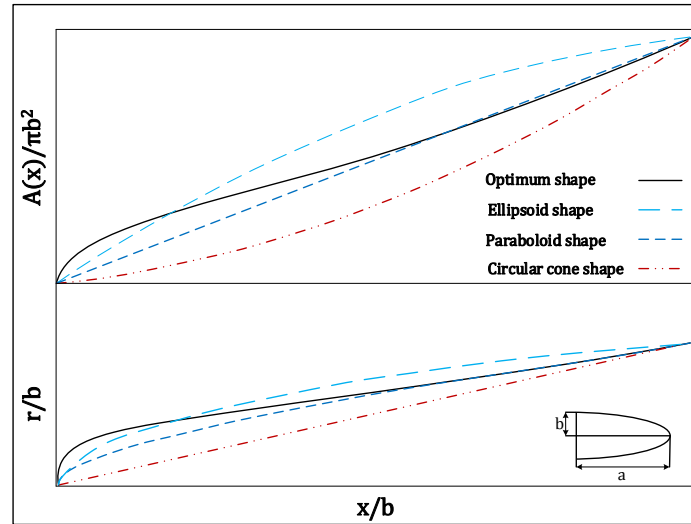


Fig. 2 Cross-sectional area distribution and radius distribution of optimum nose shape compared with other shapes<sup>8</sup>

Kikuchi et al.<sup>9</sup> used the Iida's model to modify the base shape of a paraboloid of revolution when investigating the influence of head shape on the micro-pressure wave. It was proved that the numerical pressure values of the obtained optimum shape are in a good agreement with the wind tunnel results. The comparison between the numerical calculation results and experimental results without hood in the tunnel is displayed below.

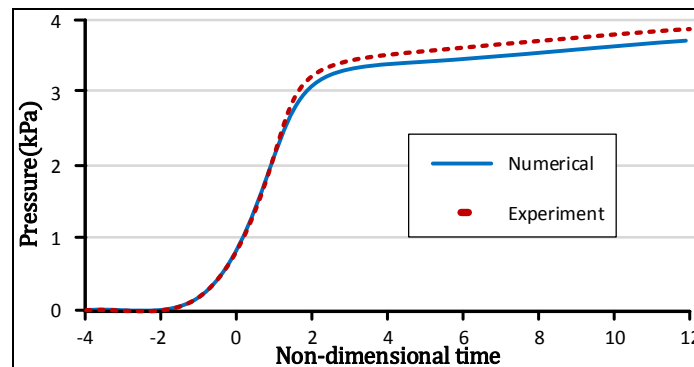


Fig. 3 Comparison of numerical calculation results with experimental results<sup>9</sup>

The parameterized model proposed by Iida only has two design variables. Simplicity and high efficiency are the two advantages of this model. The limitations are: some detail parts such as cowcatcher and driver's cab cannot be described by the model and the aerodynamic performance at the side parts cannot be analyzed. Therefore, this model is not suitable for building a complex HST head.

*The Hicks-Henne function.* The micro pressure wave is generated when the train passes through the tunnel which limits the further improvement of the train speed. The head shape can be optimized to reduce the micro pressure wave. To do this, the geometry of the head shape must be first defined with the contour line function.

In general, a polynomial expression or a composition of analytic expressions can be used as the contour line function of the train head. However the adjustment at local parts of the contour line represented with a polynomial expression does not show a satisfying effect. In contrast, the composition of analytic expressions looks better in controlling the deformation and smoothing the contour lines. Therefore, the coordinates of the points on the contour lines were expressed by Kwon et al.<sup>12</sup> as the following linear composition of the original coordinates and the perturbation values

$$Y = Y_{base} + \sum_{i=1}^6 W_i F_i, \quad (2)$$

where  $Y_{base}$  is the baseline function.  $F_i$  and  $W_i$  stand for the Hick-Henne shape function and the weighting factor, respectively. The Hick-Henne shape function  $F_i$  is described in the following Equations and presented in Fig. 4.

$$\left\{ \begin{array}{ll} F_1 = \frac{x(1-x)}{e^{20x}} & 0 < W_1 < 0.12 \\ F_2 = \sin(\pi x^{0.25})^3 & 0.03 < W_2 < 0.15 \\ F_3 = \sin(\pi x^{0.5})^3 & 0.01 < W_3 < 0.1 \\ F_4 = \sin(\pi x^{0.8})^3 & -0.05 < W_4 < 0.05 \\ F_5 = \sin(\pi x^{1.357})^3 & -0.06 < W_5 < 0.04 \\ F_6 = \sin(\pi x^3)^3 & -0.06 < W_6 < 0.04 \end{array} \right. \quad (3)$$

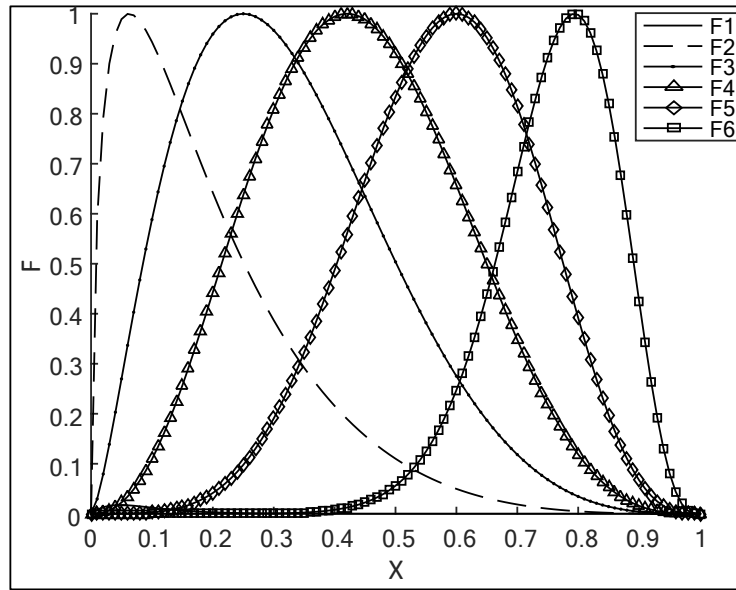


Fig. 4 Distribution of the shape functions

In order to select an appropriate baseline function, three groups of baseline functions: ellipsoid, paraboloid and cone were designed. It was found that the model using the paraboloid function could reduce the pressure gradient more effectively. Due to this reason, Lee et al.<sup>13</sup> chose the Hick-Henne model with a paraboloidal baseline to optimize the head shape of HSTs.

The Hick-Henne model was also combined with the Iida model by Ku et al.<sup>10, 14</sup> and Zhao et al.<sup>15</sup> to control the deformation of the contour lines. The combined model is described by

$$A(x) = A_{base} + \sum_{i=1}^6 W_i F_i$$

$$A_{base}(x) = \pi b^2 (1 - \alpha_2) \left[ (1 - \alpha_1) \frac{s}{a} + \alpha_1 \sqrt{\frac{s}{a}} \right] + \alpha_2 \left( \frac{s}{a} \right)^2. \quad (4)$$

The characteristics of each variable have the same meaning as the original method. The

range of  $W_i$  and the deformation of  $F_i$  are presented in Equation (3). The curvatures of the front end and the rear section on the contour line are controlled by the shape function  $F_1$  and  $F_6$ , respectively.

The optimized contour lines of Iida's model, Lee's model and Ku's model are illustrated in Fig. 5. The horizontal axis and the vertical axis correspond to the dimensionless head length and cross-section areas of the HST respectively.

The optimized Ku's model has a blunter front compared with Iida's shape and Lee's shape. In the middle section of the train head, there is no negative gradient for Iida's shape and Lee's shape because their cross-section areas are gradually increasing from the front to the rear section. However, the gradient of Ku's shape is changed from a positive gradient to a negative one, which will expand the air around the train nose, and a big pressure wave will be divided into two small pressure waves which will reduce the micro pressure wave a lot when the train enters a tunnel.

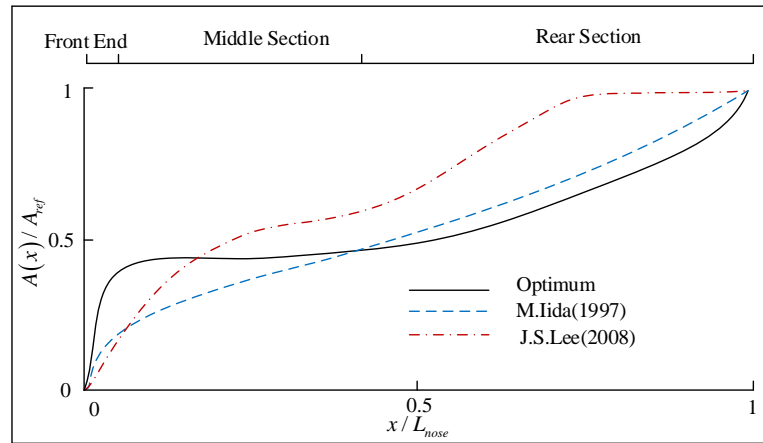


Fig. 5 The comparison of Ku's optimum shape, Iida's shape and Lee's shape

Since the Iida's model and the Hick-Henne function are combined in Ku's model that increases the number of variables and provides more degrees for head shape design, Ku's model has an ability to adjust the detailed parts of the contour lines. As a result, the intensity of the micro-pressure wave is reduced by 18-27% when compared to the parabolic shape, and by 12-19% when compared to the Iida's shape<sup>10</sup>.

*The Idealised train Model.* Chiu et al.<sup>17</sup> developed the idealised train model to study the influence of the head shape on the aerodynamic performance when the wind comes from different directions. This model, used by Hemida and Krajnović<sup>6</sup>, has a slenderness ratio of a given value and its cross-sectional profile is defined by the following equation

$$|y|^n + |z|^n = c^n, \quad (5)$$

In the above equation,  $c = \frac{h}{2}$ ,  $h$  is the height of the train head, and the value of the curvature  $n$  is determined by<sup>18</sup>

$$n = \frac{2-q}{b} z + q, \quad (6)$$

where  $q$  is the curvature coefficient of the train body and  $b$  is the length of the train head.

The contour line function describing the shape of the front from a side view is

$$\frac{z^2}{b^2} + \frac{y^2}{c^2} = 1. \quad (7)$$

The designed constraints are  $0.64h \leq b \leq 1.28h$  and  $4 \leq n \leq 6$ , and the cross-sectional profile and the length of the train head are controlled by two variables  $b$  and  $c$  respectively.

The side view and the front view of the HST are shown in Fig. 6.

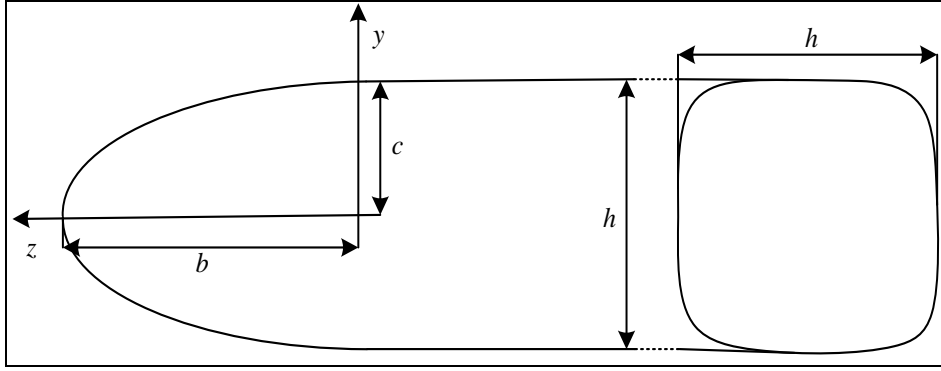


Fig. 6 The side view and front view of Idealized train model

*The 2D elliptic curve model.* In order to investigate the aerodynamic drag and the noise of the running train, Vytla et al.<sup>20</sup> and Lorriaux et al.<sup>19</sup> selected five parametric variables  $a, b, c, \theta_t$  and  $\theta_b$  to control the shape of the train head efficiently. Two elliptic curves were used to form the contour lines of the train head. The two length parameters  $a$  and  $b$  are designed to control the length of the top and the bottom elliptic curves, the height parameter  $c$  is used to change the height of the train head, and the two angle parameters  $\theta_t$  and  $\theta_b$  are used to control the bluntness of the nose shape. The shape of the 2D elliptic curve model is shown in Fig. 7 and the ranges of the five variables are defined by

$$\begin{cases} 6 \leq a \leq 7.25 \\ 1.25 \leq b \leq 2.75 \\ 0.75 \leq c \leq 1.25 \\ 0 \leq \theta_b \leq 20 \\ 0 \leq \theta_t \leq 50 \end{cases} \quad (8)$$

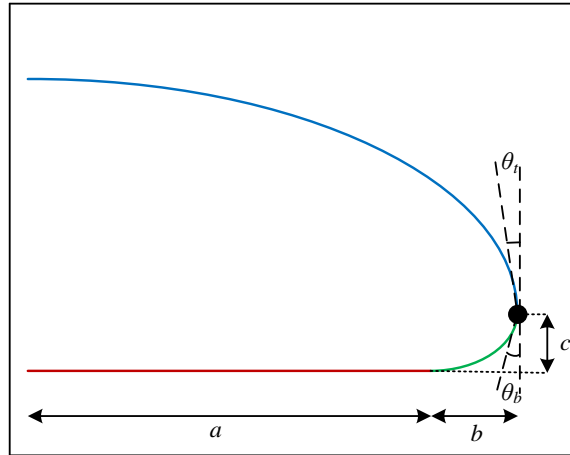


Fig. 7 The parameters of the simple 2-D elliptic curve model

*The Bézier curve model.* Muñoz-Paniagua<sup>21</sup> replaced the Hicks-Henne shape functions with Bézier curves to define the parametric contour lines of the train head and used this contour line to analyze the aerodynamic performance of the train. The function for the Bézier curve of degree  $n$  is given by

$$C(t) = \sum_{i=0}^n \binom{n}{i} (1-t)^{n-i} t^i P_i, \quad (9)$$

where  $t \in [0,1]$  is a parameter and  $\{P_i\}$  are the control points.

The train head was divided into four parts respectively defined by connecting two quadratic Bézier curves and two cubic Bézier curves with total 11 control points from  $P_0$  to  $P_{10}$  as shown in Fig. 8. Ten variables were designed to control the shape of the train nose which involved two length variables ( $l_1$  and  $l_9$ ) and two angle variables ( $\alpha_1$  and  $\alpha_6$ ). In addition, six parametric variables ( $k_i, i = 2,3,4,6,7,8$ ) were designed to avoid superposition of the relative control points.

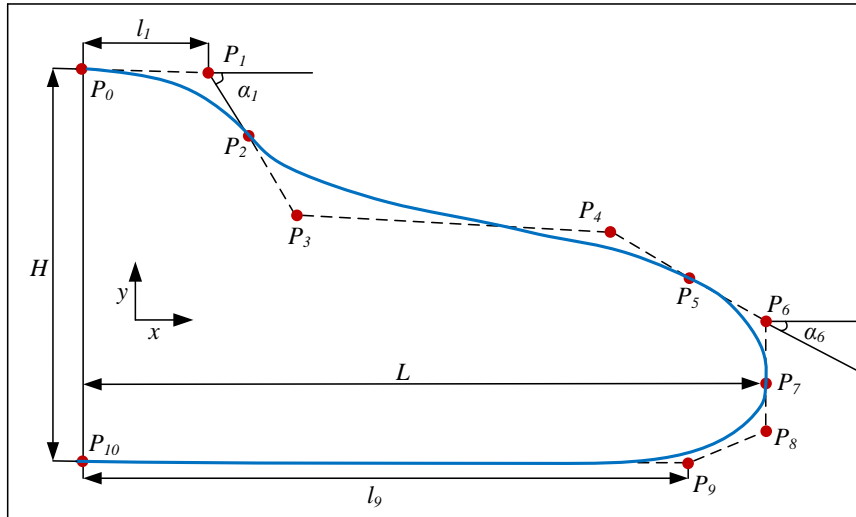


Fig. 8 The basic geometric parameters of the Bézier curve

The Bézier curve model is an effective designing technique. The expression of Bézier curve is a simple polynomial function, and the links between the controlling points and the polygons are a strong coupling relationship which can simplify the relation between the parameters and the actual design variables. Therefore, the Bézier curve model is more suitable for building a HST head comparing with the Hick-Henne model and the Iida model. Though the Bézier curve model can adjust more details on the contour line of a HST head, its designed variables are more than other methods which will take more time when optimizing the train head.

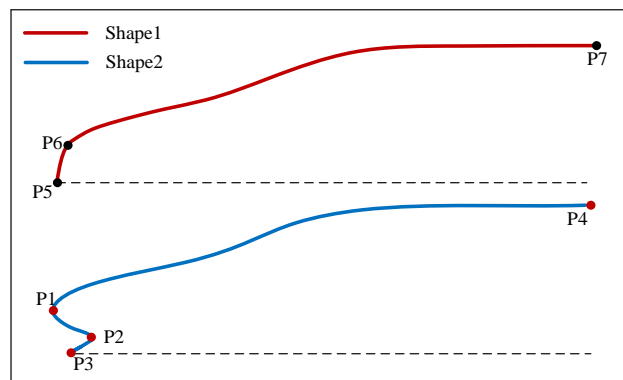


Fig. 9 The main counter line model of CRH380 series and its modified model

Here we give the two contour models in Fig. 9 to discuss the performance of each of the above mentioned methods. Shape2 in Fig. 9 is a main counter line of CRH380 series which is taken to be an original shape. Shape1 is an approximation of Shape2. The difference between the two shapes is the cowcatcher below the nose of the train head. As Tian<sup>2</sup> pointed out, the cowcatcher is needed for an optimal train head, because this part will stop the flow from going through the bottom of the train head and guide it to flow at two sides, which will improve the aerodynamic performance of the model.

The Iida's model and the Hick-Henne model can describe the Shape1 rather than the Shape2. Especially, the part from P1 to P3 of Shape2 cannot be described by the Iida's model and the

Hick-Henne model. The Idealised model and the 2D elliptic model cannot describe the shape of the whole train head shown in Fig. 9, because the main profiles of the two models are elliptic curves which cannot low its rear part down while maintaining its elliptic feature. The result of Lee's experiment shows that the model with a rear part like Shape1 and Shape2 have a better aerodynamic performance than that with a middle part described by elliptic curves<sup>13</sup>. So the Idealised model and the 2D elliptic curve model are not the best choices to design the high-speed train head. The given Shape2 can be better expressed by the Bézier curve model whilst an angle variable is added at the P2 position.

The modelling methods involved in this section have its own advantages and disadvantages comparing to other models. The main advantage for these methods is very few design parameters which contribute to high computational efficiency. The main disadvantage is simple descriptions which only present 2D contour lines rather than 3D detailed parts of the train head so that they cannot handle actual situations accurately.

### 3D parametric modelling methods

Three-dimensional (3D) parametric modelling methods use several main contours in different views to define 3D train head models. Since the train head has a symmetrical shape, only half of the train head model is generated from the main contours to raise the modelling efficiency. In this subsection, we will review three parametric modelling methods: the improved Hick-Henne function method, the vehicle modelling function (VMF), the combination of VMF and NURBS, and the combination of B-spline curves and Coons patches.

*The improved Hick-Henne function method.* Xiong et al.<sup>16</sup> improved the traditional Hick-Henne function model by using four main controlling lines (C1-C4) and five auxiliary curves (AC1-AC5) shown in Fig. 10 to build the side part of the train head. 106 control points are distributed on these curves to control the deformation of the train head.

As shown in Fig. 10, the four main controlling lines C1, C2, C3 and C4 are used to control the upper parts of the longitudinal contours, the lower parts of the longitudinal contours, the transverse profiles, and the horizontal contours, respectively. AC1 and AC2 are the auxiliary lines of the nasal tip, AC3 and AC4 are horizontal auxiliary lines, and AC5 denotes the auxiliary profiles.

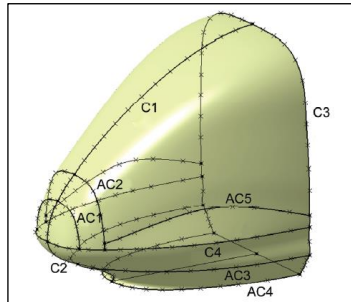


Fig. 10 Train head model and control lines<sup>16</sup>

By modifying the Hicks-Henne model, the new coordinate values of the control points are determined by the superimposing deformations on the original coordinate values

$$y_{new}(x) = y_{old}(x) + \sum_{i=1}^N w_i f_i(x), \quad (10)$$

where the functions  $f_i(x)$  are

$$f_i(x, m, n) = \sin^n(\pi x^{\ln(0.5)/(\ln(m))}). \quad (11)$$

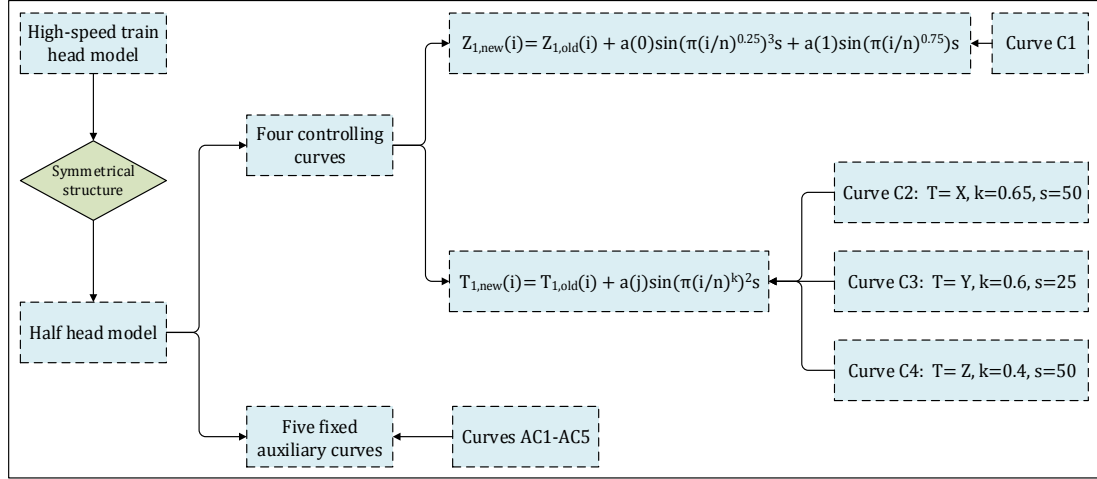


Fig. 11 The flow chart of the improved Hick-Henne function method

The flow chart of the improved Hick-Henne function method is shown in Fig. 11. As shown in the figure above, the mathematical equation for the main control line C1 is

$$Z_{1,new}(i) = Z_{1,old}(i) + a(0) \sin \left( \pi \left( \frac{i}{n} \right)^{0.25} \right)^3 s + a(1) \sin \left( \pi \left( \frac{i}{n} \right)^{0.75} \right) s, \quad (12)$$

where  $Z_{1,old}(i)$  is the original coordinate value in the  $Z$  direction and  $Z_{1,new}(i)$  is the corresponding coordinate value after deformation.  $a(0)$  is used to control the vertical nose shape,  $a(1)$  is used to control the vertical convex features of the contour lines,  $n$  is the number of points on the control lines, and  $s$  is an amplification coefficient.

The figure above also shows the mathematical equations of the main control lines C2, C3 and C4 as below:

$$T_{j,new}(i) = T_{j,old}(i) + a(j) \sin \left( \pi \times \left( \frac{i}{n} \right)^k \right)^2 s \quad (j = 2,3,4). \quad (13)$$

In the Equations above,  $T$  represents the direction where deformations of the controlling points occur.  $T_{j,old}(i)$  is the original coordinate value in the  $T$  direction and  $T_{j,new}(i)$  is the corresponding coordinate value after deformations occur. Actually, the deformed directions of counter lines C2, C3 and C4 are in  $X$  direction,  $Y$  direction and  $Z$  direction, respectively.  $\{a(j), j = 2,3,4\}$  are the designed variables, and  $k$  and  $s$  are two constant parameters.

Xiong's method is an improvement of the Hick-Henne model which selects elementary functions as its baseline, and then the superimposed exponential function is used to act as a disturbance to control the shape of the train head. Since the four main control lines and five auxiliary profiles with total 106 points are used to control the deformation of the half train head, the shape of the train head is close to the real train. The simulation results show that the maximum aerodynamic drag of the optimal train is reduced by 17.5%, and the maximum roll moment of the train head under the crosswind is reduced by 22.9% compared with the original model. Therefore this method can generate a good approximated model for the simulation of the HST head.

*The Vehicle Modelling function (VMF).* Ku et al.<sup>14</sup> proposed a two-step method to optimize the head shape of HSTs. In the first step, the cross-section area distribution is optimized to minimize the micro-pressure wave. After that, a new vehicle modelling function (VMF) is proposed to generate a parametric head model. The VMF has the form of

$$Z(x) = \frac{H}{L^{A_1+A_2}} (x - x_p)^{A_1} [2L - (x - x_p)]^{A_2} + z_p, \quad (14)$$

where  $x_p$  and  $z_p$  are the coordinates of the initial points,  $L$  describes the head length,  $H$

represents the head height, and the designed variables  $A_1$  and  $A_2$  control the bluntness of the curve.

In order to generate two-dimensional head shapes of HSTs such as side view shape, top view shape, and cross-section shape, the five steps shown in Fig. 12 are carried out.

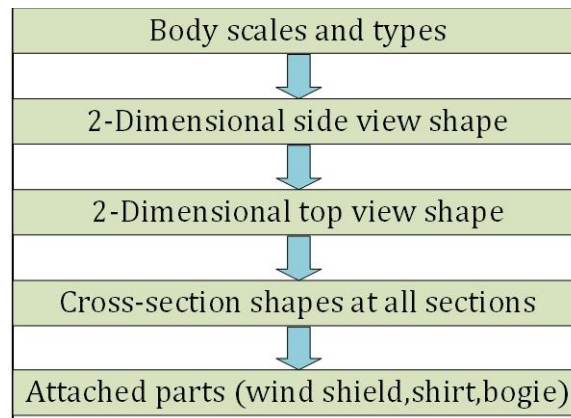


Fig. 12 Five steps of the VMF method

This method has two advantages. First, it only uses two parameters  $A_1$  and  $A_2$  to control the deformation of a simple curve. Second, it is possible to modify the head shape but still keep the given cross-sectional area distribution which minimizes the micro-pressure wave. As a result, the aerodynamic drag of the optimized 3D model is reduced by 5.6% while preserving the minimum micro-pressure wave compared with the original model.

In order to make the aerodynamics shape of the train head well described, the improved VMF is proposed by Yao et al.<sup>32</sup> to represent the 3D contour lines of the HST head. As shown in Fig. 13, 7 profile lines separated by 9 control points are used to define the HST head. The simulation results indicate that the total aerodynamic drag of the optimal train and the aerodynamic lift of the trailer train are dropped by 1.6% and 29.74% respectively in comparison with the original shape.

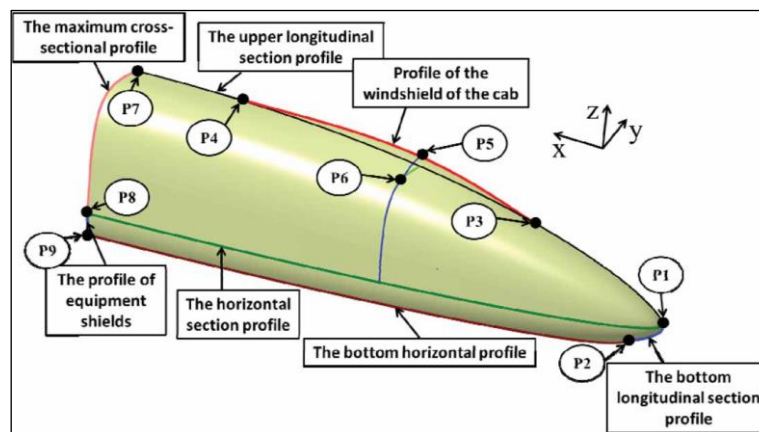


Fig. 13 Profile lines and control points in the modified VMF model<sup>32</sup>

*The combination of the VMF and NURBS.* Because of the fact that the parametric adjustment of the VMF modelling method for the complex curve is not ideal and the shape of the cowcatcher and other parts cannot be designed, Yao et al.<sup>33</sup> combined NURBS with the VMF to get the parametric model of the HST head. In Yao's model, the final train head shape is constructed by three parts of the train such as the simple shape, the cab window and the drainage. The simple shape is fitted by five profiles, the cab window and the drainage are controlled by two shape functions respectively. So the flow chart of the combination of the VMF and NURBS is shown in Fig. 14.

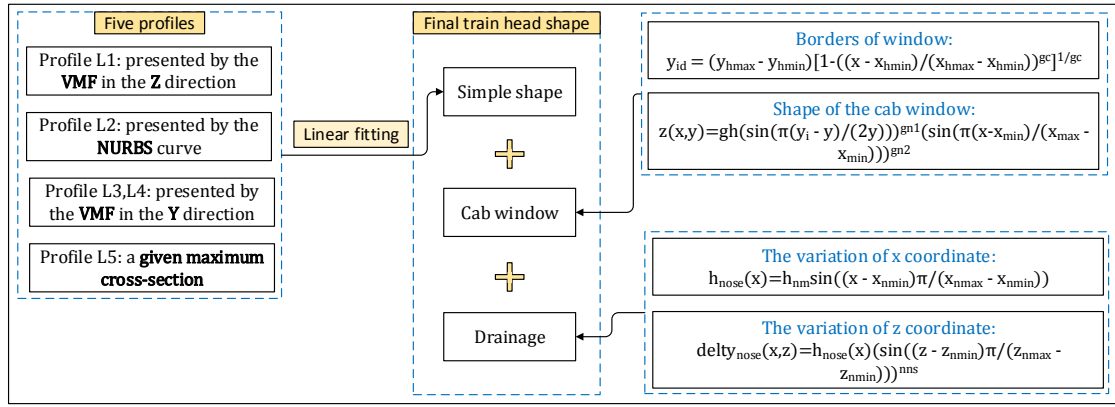


Fig. 14 The flow chart of the combination of the VMF and NURBS

As shown in Fig. 14, the five profiles are used to describe the left part of a train head because it is a symmetrical structure. The positions of these profiles are shown in Fig. 15 where L1 controls the shape of the longitudinal profile, L2 controls the contour of the train cowcatcher, L3 and L4 control the horizontal profile and bottom profile respectively, and L5 controls the maximum cross-section profile. Normally, the maximum cross-section profile has been given. Therefore, L5 will not be controlled by designed variables. Since the shapes of L1, L3 and L4 are simple, they can be designed by using the VMF method. L3 and L4 have a similar VMF expression because the shape of the described profiles is very similar. L2 controls the complex shape of the cowcatcher. So a three-order NURBS curve with 5 control points is used to control this profile.

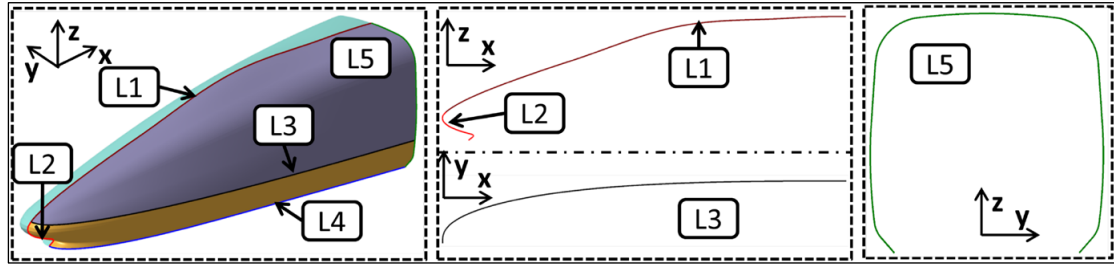


Fig. 15 The contour line of the train head<sup>33</sup>

In order to describe the profile of the train head and control the curvature of contour lines, Yao et al. modified the VMF model as follows:

$$F\left(\frac{x}{c}\right) = \left(\frac{x}{c}\right)^{A_1} \left(1 - \frac{x}{c}\right)^{A_2} S\left(\frac{x}{c}\right) + G\left(\frac{x}{c}\right), \quad (15)$$

where  $G\left(\frac{x}{c}\right)$  controls the curvature at the end of the curve which is mostly expressed as a polynomial, and the coefficients of the polynomial are determined by the coordinate values and the curvature of the points at the end of the curve.

The equation of the profile L1 is represented by

$$z(x) = \left(\frac{x-x_{11}}{x_{12}-x_{11}}\right)^{A_{11}} \left(1 - \frac{x-x_{11}}{x_{12}-x_{11}}\right)^{A_{12}} a_{k1} \left(1 - \frac{x-x_{11}}{x_{12}-x_{11}}\right)^{a_{b1}} + g(x), \quad (16)$$

$$g(x) = 2(z_{12} - z_{11}) \frac{x-x_{11}}{x_{12}-x_{11}} - (z_{12} - z_{11}) \left(\frac{x-x_{11}}{x_{12}-x_{11}}\right)^2$$

where  $g(x)$  is designed to control the height and the curvature of endpoints,  $x_{11}$  and  $x_{12}$  represent the coordinate values of the starting point and the end point respectively in the X direction.  $z_{11}$  and  $z_{12}$  represent the coordinate values of the starting point and the end point respectively in the Z direction.

L2 controls the profile of the cowcatcher, and it is designed by NURBS curves as shown in Fig. 16. In addition, a quadratic polynomial is attached to the NURBS curve to control the length of the streamline which is given as

$$\begin{aligned} x(z) &= p_x(u) + g(z) \\ g(z) &= A(z - H)^2 + B' \end{aligned} \quad (17)$$

where  $p_x(u) \geq 0$ , and  $H$  is the value of  $z$  when  $p_x(u) = p_{min}$  ( $p_{min} > 0$ ). The parameter  $A$  which controls the width of the polynomial is determined by the coordinate of the control point P5 in the  $X$  direction.  $B$  is determined by the coordinate of the control point P1 in the  $X$  direction. In order to reduce the number of design variables, the weights in the Equations above are set as a simple constant.

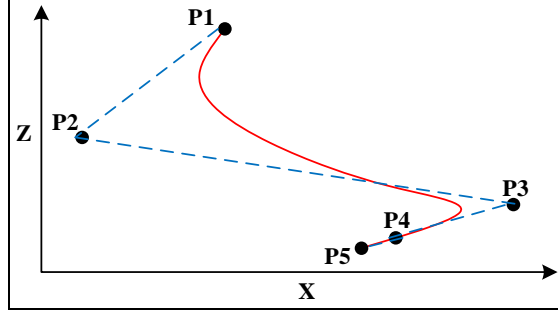


Fig. 16 The cowcatcher designed with NURBS

L3 and L4 have a similar form which are given by

$$\begin{aligned} y(x) &= \left( \frac{x-x_{21}}{x_{22}-x_{21}} \right)^{A_{21}} \left( 1 - \frac{x-x_{21}}{x_{22}-x_{21}} \right)^{A_{22}} a_{k2} \left( \frac{x-x_{21}}{x_{22}-x_{21}} - 1 \right)^{a_{b2}} + g(x) \\ g(x) &= 2(y_{22} - y_{21}) \frac{x-x_{21}}{x_{22}-x_{21}} - (y_{22} - y_{21}) \left( \frac{x-x_{21}}{x_{22}-x_{21}} \right)^2 \end{aligned}, \quad (18)$$

where the meaning of  $g(x)$  and other variables are same as those in Equations (16).

The head shape of the HST is controlled by several 2D profiles, and the deformation of the train head is driven by changing the shape of these curves. Each surface on the train head is treated as a spatial quadrilateral. 20 variables are designed to control the deformation of the train head. The coordinate values of the 20 points on the surfaces of the train head can be obtained by using a linear fitting model below

$$\begin{aligned} y(x) &= y_{min}(x) + \frac{x}{l(x)} y_{max}(x) \\ z(x) &= z_{min}(x) + \frac{x}{l(x)} z_{max}(x) \end{aligned} \quad (19)$$

As shown in Fig. 14, the shape of the cab window is determined by

$$\begin{aligned} y_{id} &= (y_{hmax} - y_{hmin}) \left[ 1 - \left( \frac{x-x_{hmin}}{x_{hmax}-x_{hmin}} \right)^{gc} \right]^{\frac{1}{gc}}, \\ z(x, y) &= gh \left( \sin\left( \frac{\pi(y_i - y)}{2y} \right) \right)^{gn1} \left( \sin\left( \frac{\pi(x-x_{min})}{x_{max}-x_{min}} \right) \right)^{gn2} \end{aligned}, \quad (20)$$

where  $y_{id}$  determines the coordinates of the borders, the parametric  $gc$  controls the shape of the borders,  $z(x, y)$  controls the shape of the cab window,  $gh$  controls the height of the window, and  $gn1$  and  $gn2$  control the transition between the cab window and the simple shape.

The shape of the drainage is obtained by controlling the coordinate values at the  $Y$  axis, which are determined by

$$h_{nose}(x) = h_{nm} \sin\left(\frac{x-x_{nmin}}{x_{nmax}-x_{nmin}}\pi\right)$$

$$delty_{nose}(x,z) = h_{nose}(x) \left(\sin\left(\frac{z-z_{nmin}}{z_{nmax}-z_{nmin}}\pi\right)\right)^{nns}, \quad (21)$$

where  $h_{nose}(x)$  controls the variation of the drainage in the  $X$  axis,  $h_{nm}$  is the maximum variation,  $delty_{nose}(x,z)$  describes the variation in the  $Z$  axis, and  $nns$  controls the smoothness of the transition between the drainage and the simple shape.

Since the obtained quadrilateral surfaces could not be jointed smoothly, Yao et al. used Laplace smoothing method to deal with this issue. The surfaces of the train head are divided into three parts: simple shape, the cab window and the drainage. Each parts of the train head has its own controlling functions, and 13 parameters are used to control the surface deformations of the train head. The whole parametric design process of the train head is shown in Fig. 17.

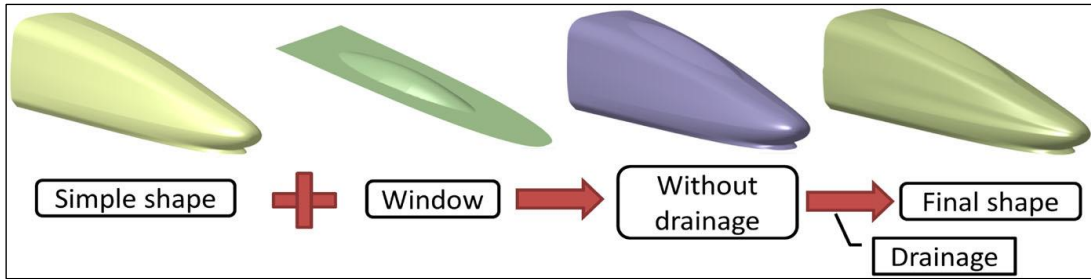


Fig. 17 The process of parametric design of the train head<sup>33</sup>

This method makes the constructed model closer to the real one since it takes the cab window and the drainage into consideration. The simulation results indicate that the total aerodynamic drag of the optimal train is reduced by 13.62%, and the aerodynamic lift is reduced by 9.84% compared with the real train model. However, 30 parametric variables are involved in the whole modelling process which makes this method less efficient.

*The combination of the B-spline curves and Coons patches.* Suzuki<sup>22</sup> studied the aerodynamic properties of the high-speed train head by combining the B-spline curves and Coons patches. In order to generate the 3D shape of the high-speed train head, three steps shown in Fig. 18 are carried out.

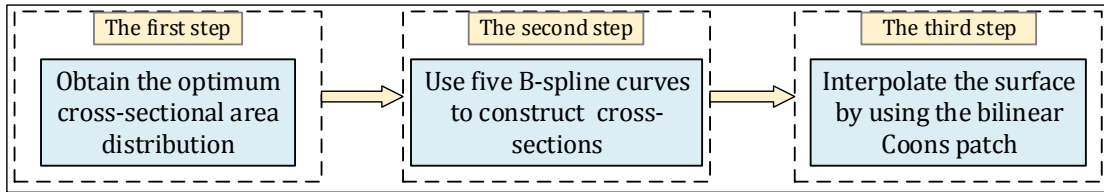


Fig. 18 Three steps to construct a 3D high-speed train head

Bellenoue<sup>11</sup> pointed out that the optimized distribution of the cross-sectional area can be used as a guideline for the design of 3D head shape described as the first step in the figure above. Therefore, the optimum cross-section area variation is obtained as a constraint condition for the 3D train head shape. Meanwhile, Equation (1) is used to define the cross-section area. In the second step, five third-order B-spline curves are involved to define the cross-sections based on the obtained optimum cross-sectional area distribution. The head shape and the cross-sections are shown in Fig. 19. In the Fig. 19.b, four control points are used to define one B-spline curve, and the distance  $d$  is set to be a constant for reducing the computational cost. In the third step, the bilinear Coons patches are used to interpolate the surface between two adjacent cross sections which are shown in Fig. 19.a. Since the optimum cross-section area distribution is obtained before creating the head shape in the first step and the design variables are not needed in the third step, only five design variables in the second step are used to build the train head shape.

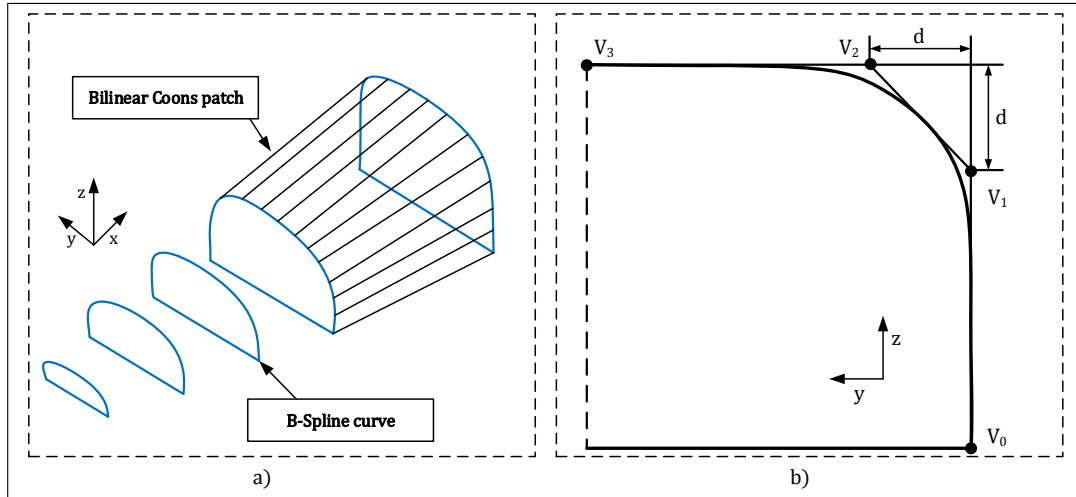


Fig. 19 a) representation of train head shape; b) Definition of cross-section by third-order B-spline curve

Although this method combines the B-spline curve and the optimum cross-section area distribution, the shape of the train head is actually controlled by five B-spline curves. If more control points are involved in the B-spline curves, this method will better control the head shape of the high-speed train since five design variables cannot define some detail parts.

#### *CATIA-based parametric modelling methods*

CATIA-based parametric modelling methods use some parameters or parametric descriptions of head shapes and the software CATIA to generate 3D models of HST heads. In this subsection, we will review two CATIA-based parametric modelling methods: CATIA-based three-parameter method, and CATIA-based B-spline curve method. The former designs the parameters for the train head by using the software CATIA directly. Although this method can generate 3D head shapes and control some main areas, it cannot describe some local parts since only three parameters are used. The latter generates parametric models from the macro recording of the CATIA software, approximates main profile lines with B-spline curves, and deforms the train head by adjusting the shape of these profile lines.

*CATIA-based three-parameter method.* Muñoz-Paniagua and Crespo<sup>23</sup> used the software CATIA to create the geometry of the train head and used three parameters  $l_1$ ,  $l_2$  and  $R_1$  shown in Fig. 20 to control shape changes of the train head. The variable  $l_1 \in [w, 4w]$  controls the contraction of the nasal tip and  $w$  is the train width. The total length of the train head  $L$  is set as a constant. The parameter  $l_2 \in [\frac{1}{6}w, \frac{1}{3}w]$  is used to adjust the bluntness of the train nose, and  $R_1 \in [\frac{1}{6}w, \frac{1}{3}w]$  is used to change the cross-section area of the train head and the bluntness of the nose tip. The height parameter  $H$ , the width parameter  $w$ , the bluntness parameter  $r_t$  and the connection parameter  $r_c$  shown in the Fig. 20 are all set as constants. The simulation experiments are designed to study the effects of the train head length, nose bluntness and blocking on the aerodynamic performance of the HST.

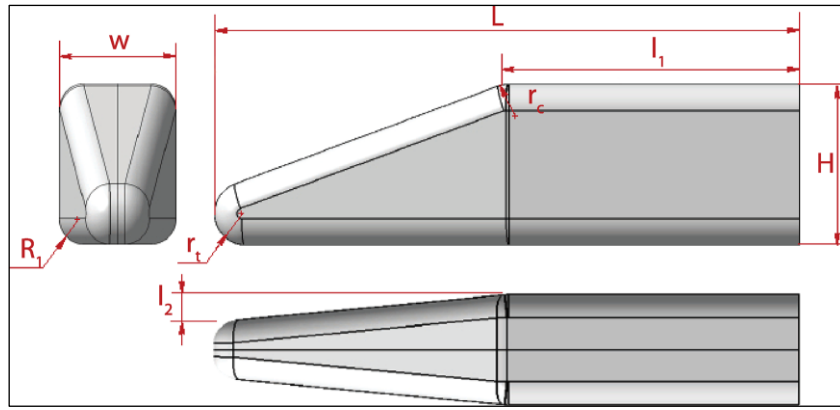


Fig. 20 The geometric parameters of the CATIA-based three-parameter method<sup>23</sup>

The whole head shape generated by the three-parameter method is similar to the actual train head shape. Since only global factors such as the length, width, nose height and nose bluntness are considered, local details such as the drain, driver cab and cowcatcher have not been designed by this modelling method. So the models generated by this method are very limited.

*CATIA-based B-spline curve method.* The high speed train head shape is very complex. The three parameters  $l_1, l_2$  and  $R_1$  cannot describe such complexity. Therefore Yu<sup>24,25</sup> and Li<sup>26</sup> established the 3D model with CATIA and generated a VBscript by using the macro recording function of the CATIA, then the left part of this model was generated with the script because the train head had a symmetrical structure. Finally the deformation of the train head was controlled by modifying the script of the CATIA with the software MATALB. 162 control points are used to generate 12 B-spline curves C1 to C12 and 7 B-spline surfaces which are shown in Fig. 21 where X, Y, and Z indicate longitudinal, horizontal, and vertical directions, respectively.

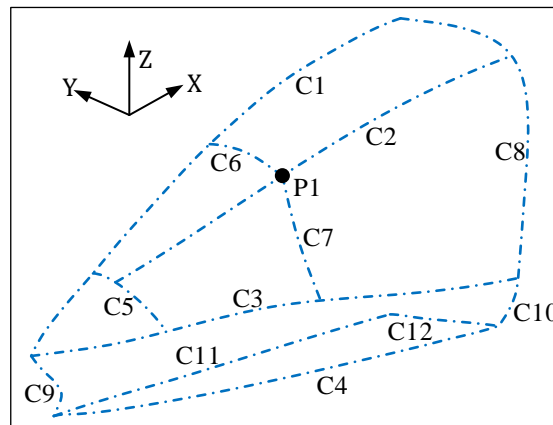


Fig. 21 The left part of the train head

In order to optimize the shape of the HST, five variables  $dz_1, dy_3, dy_4, dy_7$  and  $n_\tau$  shown in Table 1 are designed to control the contour lines C1, C3, C4, C7 and C9. How these variables influence the five control lines are also given in this table.

The variations of the vertices on the spline curves C1, C3 and C4 have the same form. The coordinates of the vertices on C1 are changed in the vertical direction Z, and the coordinates of the vertices on C3 and C4 are changed in the horizontal direction Y. The changes are the maximum at the middle point indicated by  $dz_1, dy_3$  and  $dy_4$  among which  $dz_1$  for C1 and  $dy_3$  for C3 have been indicated in Fig. 22. The red dashed curve, black solid curve, and blue dashed curve depicted in the left one of Fig. 22 indicate the upward movement ( $dz_1 > 0$ ), the original shape, and the downward movement ( $dz_1 < 0$ ) of the spline curve C1. Similarly, the red dashed curve, black solid curve, and blue dashed curve depicted in the right one of Fig. 22 demonstrate the outward movement ( $dy_3 < 0$ ), the original shape, and the inward movement ( $dy_3 > 0$ ) of the spline curve C3. For the points between the middle and the two end points, the

changes follow a linear interpolation. That is to say, the changes linearly reduce from the maximum at the middle point to zero at the two end points.

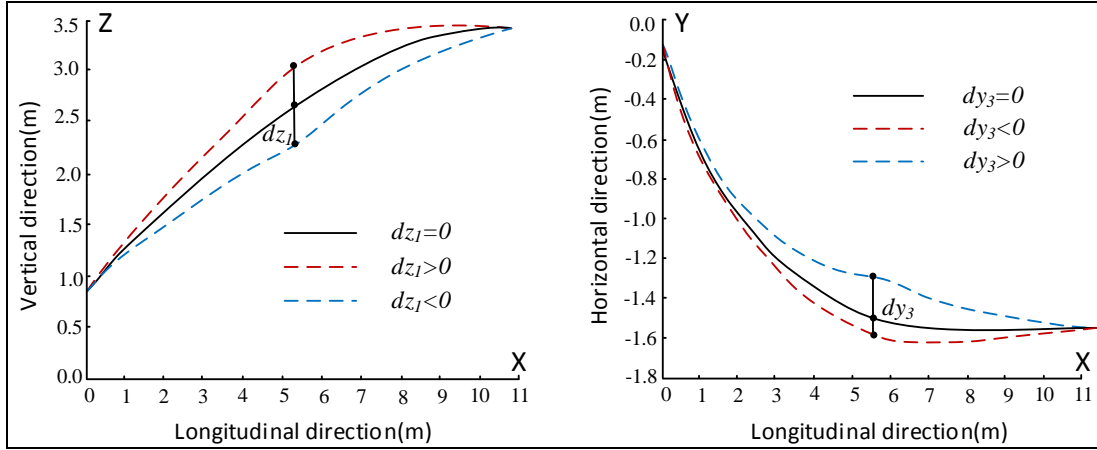


Fig. 22 Deformation of the longitudinal symmetry lines C1 and C3

The deformations of the control line C7 are mainly the changes of convexity which can be defined by the following equation

$$y_{7,new}(i) = y_{7,old}(i) \left( 1 + \frac{dy_7(i-1)(n_7-i)}{(i-1)(i-1)+(n_7-i)(n_7-i)} \right), \quad (22)$$

where  $y_{7,old}(i)$  and  $y_{7,new}(i)$  are the coordinates of the points before and after the deformation occurs,  $i$  is the serial number of the points on C7,  $n_7$  is the number of the control points on C7, and  $dy_7$  is the designed variable.

In order to control the height of the nose, the coordinates of the points on C9 are multiplied by the coefficient  $n_\tau$ . Clearly,  $n_\tau > 1$ ,  $n_\tau = 1$  and  $n_\tau < 1$  will lead to a larger, unchanged, and smaller nose height, respectively.

Table 1 Design variables and their influences

Variables	Control line		influences
$dz_1$	Control line C1	$dz_1 > 0$	the upward movement of C1
		$dz_1 = 0$	C1 remains unchanged
		$dz_1 < 0$	the downward movement of C1
$dy_3$	Control line C3	$dy_3 > 0$	the body becomes narrower
		$dy_3 = 0$	the body remains unchanged
		$dy_3 < 0$	the body becomes wider
$dy_4$	Control line C4	$dy_4 > 0$	the bottom becomes narrower
		$dy_4 = 0$	the bottom remains unchanged
		$dy_4 < 0$	the bottom becomes wider
$dy_7$	Control line C7	$dy_7 > 0$	the upward movement of C7
		$dy_7 = 0$	C7 remains unchanged
		$dy_7 < 0$	the downward movement of C7
$n_\tau$	The nose height	$n_\tau > 1$	the nose becomes higher
		$n_\tau = 1$	the nose remains unchanged
		$n_\tau < 1$	the nose becomes lower

This method controls the deformation of the train head by adjusting some key points on the profiles, and the train model is well described. After optimization, the aerodynamic drag and the load reduction factor are dropped by 4.15% and 1.72% respectively compared with the original shape. However it is difficult to ensure smooth transitions when crossing the control lines, such as the areas around the point P1 shown in the Fig. 21, because the deformations in these areas are respectively defined by the control lines C2, C6 and C7 whose changes are different.

---

### Mesh deformation-based parametric modelling methods

The mesh deformation-based methods firstly mesh the model whose shape is to be optimized. Then surface deformations are applied by moving the grid points. The deformed surfaces are  $C^1$  continuity in each modelling step. When the deformation occurs, every grid point moves simultaneously to keep the smoothness of the new surface. These methods can simplify the optimized process of complex geometries and improve the optimized efficiency. Three kinds of mesh deformation-based parametric modelling techniques are introduced in this section to design the head model of HSTs.

*The FFD-based parametric modelling method.* Applying the free-form deformation (FFD)<sup>34</sup> to deform the meshes of high-speed train heads can replace the remodeling and re-meshing step since it modifies part of grids and keeps the remaining grids unchanged. Therefore, the FFD can greatly improve the parameterization efficiency.

Li<sup>35</sup> introduced the FFD parameterization to describe the shape of a 3D train head. As shown in Fig. 23, the train head was divided into four parts. Five variables were designed to constrain the deformation of the train head with the height in the Z direction for Part 1, the height in the Z direction for Part 2, the height in the Z direction and the length in the X direction for the Part 3, and the length in the Y direction for Part 4. The deformation function at an arbitrary point was defined by a trivariate tensor product Bernstein polynomial.

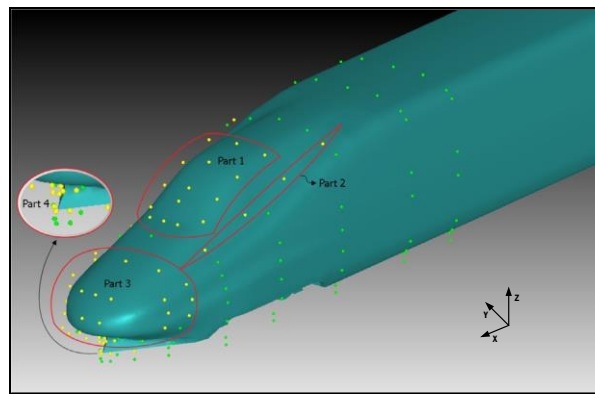


Fig. 23 The model of FFD parameterization method<sup>35</sup>

The FFD can be used to control the shape of surfaces globally or locally with derivative continuity. It is suitable for complex geometries<sup>36</sup>. In addition, it can reduce the computer consumption in the optimization process since it avoids the remodeling and re-meshing step. The simulation results show that the total drag force of the optimal model and the lift forces of the head and tail are decreased by 3.55%, 9.59%, and 10.85% respectively by comparison with the original shape. However, the local FFD generates a planar boundary with the undeformed meshes and it is quite costly to create an arbitrary boundary curve since we must start a FFD in an already deformed orientation and deform it some more<sup>34</sup>.

*Arbitrary shape deformation (ASD)-based parametric modelling method.* When using the ASD-based method, an ASD volume which contains control points and their relations is built based on the original mesh model. By moving control points in the ASD volume, the related meshes are deformed smoothly which keeps the quality of the deformations. So it becomes possible to optimize the complex geometric shapes with this technique.

Cui<sup>27</sup> was the first one who applied the ASD-based method to design the parametric model of a HST head. Yao<sup>28</sup> divided the head shape of CRH380A into five deformation regions shown in Fig. 24. The structural grid was utilized to mesh every deformation region, and then the coordinates of some special key nodes were obtained. Next the given cosine functions were used to get the coordinate increments of these particular key nodes which was based on some key points of the grids, including the connection part between the driver's cab and the top, the peak of the cowl, the peak of the nose and the maximal curvature point at the drainage area. Finally the train head was controlled by combining the coordinate's increments of these key points with the deformation function of each region.

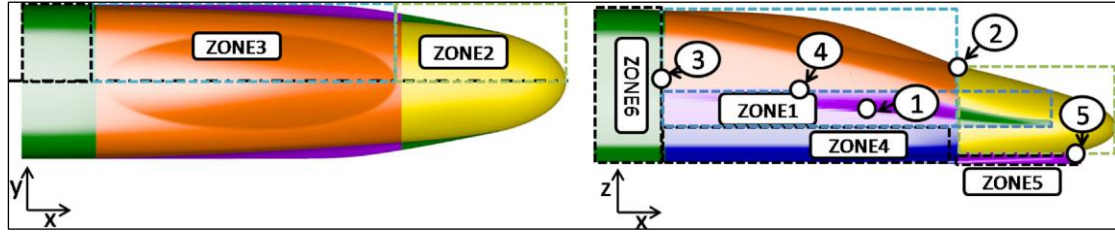


Fig. 24 Schematic diagrams of deformation zones<sup>28</sup>

The deformation functions and the designed parameters of each region are given in Table 2 where  $\Delta y$  is the increments in the Y direction,  $x_1$  and  $y_1$  are the coordinates of the key point in the X and the Y direction respectively,  $menum$  is the total number of grids in the Z direction,  $mx_1$  and  $nx_1$  control the maximal and minimal coordinates of grids respectively in the X direction, and  $my_1$  and  $ny_1$  are in the Y direction. The meanings of variables in other deformation regions are similar to those in the ZONE1.

Table 2 Deformation function and design parameters of each deformation region

Areas	Deformation function	Designed parameter	Deformation region
ZONE1	$\Delta y = w_1 \cos\left(\frac{\pi(x - x_1)}{mx_1 - nx_1}\right) \cos\left(\frac{\pi(y_1 - menum)}{my_1 - ny_1}\right)$	$w_1$	Nose drainage area
ZONE2	$\Delta z = w_2 \cos\left(\frac{\pi(x - x_2)}{mx_2 - nx_2}\right) \cos\left(\frac{\pi(z - z_2)}{mz_2 - nz_2}\right)$	$w_2$	Height of nose drainage area
ZONE3	$\Delta y = w_3 \cos\left(\frac{\pi(x - x_3)}{mx_3 - nx_3}\right) \sin\left(\frac{\pi(y - y_3)}{my_3 - ny_3}\right) \times \cos\left(\frac{\pi(z - z_3)}{2(mz_3 - nz_3)}\right)$	$w_3$	Width of the train body
ZONE4	$\Delta z = w_4 \cos\left(\frac{\pi(x - x_4)}{mx_4 - nx_4}\right) \sin\left(\frac{\pi(z - z_4)}{mz_4 - nz_4}\right)$	$w_4$	Perspective of the cab
ZONE5	$\Delta z = w_5 \cos\left(\frac{\pi(x - x_5)}{2(mx_5 - nx_5)}\right) \sin\left(\frac{\pi(z - z_5)}{mz_5 - nz_5}\right)$	$w_5$	Shape of the cowcatcher

Sun<sup>37</sup> applied the ASD-based method to build the parametric model of the CRH3 series train heads. Four parametric variables such as the height of the train head, the thickness of the nose, the length of the nose and the height of the driver's cab were designed to control the deformation of the streamlined shape.

The model generated with the ASD-based method is very close to the original shape. As a result, in the conditions without crosswind, the total drag force of the optimal train and the lift force of the trailing car are reduced by 3.34% and 27.86%, respectively, in comparison with the original model; and they are reduced by 2.1% and 5.43%, respectively, in the crosswind conditions. Furthermore, few variables are utilized to control the deformation of the HST head which shortens the time consumption of geometry regeneration and improves the efficiency of the optimization calculation.

*Local shape function-based parametric modelling method.* Henry et al.<sup>38</sup> extended FFDs by basing them on NURBS and named the extended FFDs as NURBS-based FFDs (NFFDs) which is effective in the deformation of the solids and surfaces. Yao et al.<sup>29-31</sup> developed the local shape function (LSF)-based method to design the parametric shape of the CRH380A. This method is based on the NFFDs. The implementation steps of LSF-based method are:

Step1: Discretize the deformation regions.

Step2: Use the structural grid to mesh the deformation regions.

Step3: Match the deformation functions and ensure the smoothness between two adjacent regions which are shown in Fig. 25.

Step4: Choose weight factors  $W_i$ .

Step5: Calculate the coordinate's increments  $\Delta$  with the deformation functions  $l_i$ .  
 Step6: Sum the original coordinates and  $\Delta$  to get the deformed coordinates.  
 Step7: Fit the surfaces with the deformed coordinates.

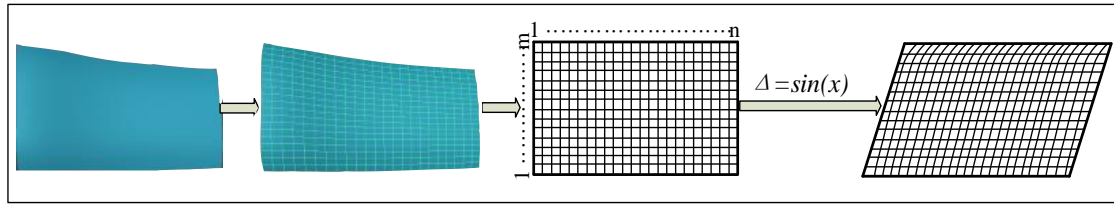


Fig. 25 Schematic of surface deformation by LSF

Yao et al. had proved that different deformation functions would generate different surfaces. Unreasonable deformation functions would produce a distorted surface, so it was very important to choose deformation functions. In general, the trigonometric function, the exponential function, the logarithmic function, the polynomial function and the NURBS function can be used as the deformation functions. In order to simplify the calculation, the trigonometric function was selected as the deformation functions in this method.

The train head of CRH380A was divided into seven deformation regions as shown in Fig. 26. The relations among the deformation regions, the control areas, the controlled points and the design parameters are shown in Table 3.

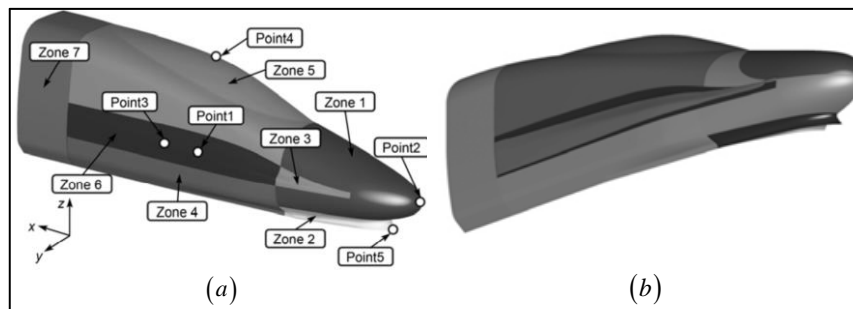


Fig. 26 Deformation zones and local deformations. a) Schematic of deformation zones; b) deformation of the nose and cowcatcher<sup>29</sup>

Table 3 The information of the design variables

deformation regions	control zones	control point	coordinate direction → design variable	variable range
Nose drainage	zone 3 , zone 6	Point1	$z \rightarrow w_1$	$-5 \leq w_1 \leq 5$
Nose height	zone 1 , zone 3	Point2	$z \rightarrow w_2$	$-15 \leq w_2 \leq 10$
The width of the streamline	zones 4 to zone7	Point3	$y \rightarrow w_3$	$-5 \leq w_3 \leq 20$
cab windows	zones 5 , zone 6	Point4	$z \rightarrow w_4$	$-10 \leq w_4 \leq 4$
cowcatcher	zone 2	Point5	$x \rightarrow w_5$	$-60 \leq w_5 \leq 10$

The original design parameters are not needed and the topological structure of grids is unchanged in the FFD-based modelling. However, the effect is not obvious when using the FFD based modelling to adjust the deformation of the local shape<sup>46</sup>. Although the NURBS based modelling can describe the whole head model, and local shapes are well controlled, a lot of control points and curves are involved, which is proved inefficient<sup>47,48</sup>. The LSF-based method was proposed to tackle the limitations of the FFDs and NURBS based modelling. The simulation results indicate that the total drag of the optimal train is reduced by 2.26% and the lift force of the trailing car is reduced by 19.67% compared with the prototype CRH380A. But the LSF-based method also has some weaknesses. It needs to calculate the movement of every grid

---

points. If the grids are divided densely, the design of the train head is inefficient. If the grids are divided sparsely, the results will be inaccurate.

## Conclusions and discussions about potential research directions

With the increasing speed of trains, some ignored aerodynamic factors at low speed have limited the improvement of the train speed. Evidences show that the head shape of the HST becomes a key point to improve its aerodynamic performance. Although the tunnel test, numerical simulations, and real vehicle tests have been used to obtain better head shapes, they are expensive and time-consuming. Parametric modelling, able to save the time and cost greatly, has become essential in the train head design.

This paper summarizes various parametric train head modelling methods which vary from a simple profile to a complex train head model. Although the calculating efficiency of 2D contour line modelling methods is fast, they mainly use one main contour line which does not provide enough information to define 3D train head models. Due to this reason, the head shape defined by 2D contour line modelling methods is very simple compared to the actual train head. Therefore these methods can hardly reflect the real condition of the running train. In contrast, 3D parametric modelling methods introduce more contour lines to define 3D train head models leading to better shape design of HST heads. However, how to describe local shape details and realistic train heads with least design variables is still an unsolved problem for 3D parametric modelling. The future research may concentrate on the following directions.

First, control contours play a dominate role in determining correct train head shapes. Properly identifying number and positions of control contours may be a research focus. One question to be answered is: do current 3D parametric modelling methods provide sufficient control contours to describe 3D shapes of HST heads accurately? If not, where the new control contours should be increased? Shape analysis of HST heads may help identify the positions and distributions of proper control contours. There are some shape analysis methods. For example, the variation of curvature of the head shape can be used to determine the positions and distribution of control contours. In the areas with small curvature values, fewer control contours should be used. In the areas with large curvature values, more control contours should be allocated.

Second, how to use few design variables to represent control contours accurately may be a potential topic, because more variables means more time consumption in the process of optimization. Although control point-based curves such as Bézier curves and NURBS curves can do the work, they may not be ideal in describing complex shapes with few design variables. New mathematical expressions which are able to describe local shapes with few design variables could be investigated to address this issue. Fourier series could be a good example in providing an effective solution to this problem. The terms of the Fourier series and Fourier coefficients can be optimally determined through curve fitting according to the required errors. For complex control contours, piece-wise Fourier series can be introduced to simplify the problem. First, each of complex control contours is divided into several simple segments. Then, a Fourier series is used to approximate each of the simple segments.

Third, develop new methods to deal with the smoothness problem between two adjacent surface patches. Currently, the treatments of this issue are to use some smoothing methods such as Laplace smoothing while each of the surface patches is generated by the control contours. However, such smoothing methods change the original shapes of the surface patches. New methods which can achieve both smooth transition between two adjacent surface patches and keep the original shapes unchanged could be developed. Ordinary differential equation (ODE)-based sweeping surfaces<sup>39</sup> have an ability to obtain any high-order continuities between two adjacent sweeping surface patches and rebuild the original surfaces with high accuracy. This is because that two adjacent ODE sweeping surfaces share the same boundary conditions. If the shared boundary conditions contain positional and first derivative functions, the two adjacent ODE surfaces will achieve  $C^1$  continuity at the boundary. If the second or higher derivatives will also be included in the boundary conditions, the two adjacent surfaces will achieve  $C^2$  or higher continuity at the boundary.

Fourth, investigate new surface patch-based 3D parametric modelling methods. In current 3D parametric modelling methods, more details of the models are described, more design variables are needed, which makes the optimization inefficient. To tackle this problem, it may be necessary to develop new surface patches which can describe complex shapes with few

---

design variables and build the whole head models of HSTs with these new surface patches. Partial differential equation (PDE)-based surface patches<sup>40</sup> are more capable in describing a complex shape with few design parameters than other surface patches such as NURBS surface patches. The complex shape shown in Fig. 27 is taken from Ref. 41 and consists of one single PDE surface patch. It is clear that a single NURBS surface patch or any other single surface patch is impossible to create the complex shape. Therefore, partial differential equation-based surface modelling could be introduced to develop a new surface patch-based 3D parametric modelling method of HST heads.

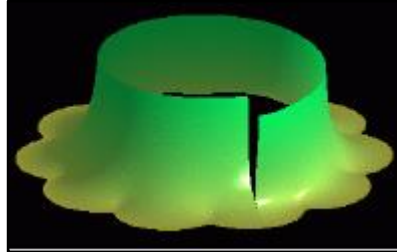


Fig. 27 Complex surface consisting of only one single patch<sup>41</sup>

Fifth, develop new coupling methods to consider the coupling effect between HSTs and roadside buildings by integrating them with 3D parametric modelling and optimization calculations to obtain the optimal shape of HST heads. Current researches on the aerodynamic performance of the train head mainly focus on one single object, such as the shape of the train head we discussed in this paper, the height and position of the wind-break wall<sup>42,43</sup>, the shape of noise barrier<sup>44,45</sup>, the height, width and cross-sectional area distribution of the bridge<sup>49</sup>, and the structure of the tunnel portal geometry<sup>50-52</sup>. However, the aerodynamic effect is an interaction of all these factors. With the continuous improvement of the running speed, the coupling effect between the train and the roadside buildings becomes more and more serious to restrict the further development of the high-speed train. Therefore, it is important to develop new coupling methods to consider the interaction among these factors.

## Acknowledgments

This research is supported by the National Natural Science Foundation of China (Grant no. 51475394), the Independent Research Project of the State Key Laboratory of Traction Power (No.2015TPL\_T06), the Fundamental Research Funds for the Central Universities (No. 2682016CX128), and EU Horizon 2020 funded project “PDE-GIR” (H2020-MSCA-RISE-2017-778035).

## References

1. RAGHUNATHAN R S, KIM H D, SETOGUCHI T. Aerodynamics of high-speed railway train. *J Progress in Aerospace Sciences* 2002; 38(6-7): 469-514.
2. TIAN H Q. Train aerodynamics. *China railway publishing house*, 2007; 99-114.
3. MAEDA T, KINOSHITA M, KAJIYAMA H, et al. Aerodynamic drag of Shinkansen electric cars (series 0, series 200, series 100). *J Railway Technical Research Institute Quarterly Reports* 1989; 30(1).
4. KIKUCHI K, TANAKA Y, IIDA M, et al. Contour measures for Reducing Pressure Variation due to Train Passage in Open Sections. *J Quarterly Report of Rtri* 2001; 42(2): 77-82.
5. CHOI J K, KIM K H. Effects of nose shape and tunnel cross-sectional area on aerodynamic drag of train traveling in tunnels. *J Tunnelling & Underground Space Technology* 2014; 41:62-73.
6. HEMIDA H, KRAJNOVIĆ S. LES study of the influence of the nose shape and yaw angles on flow structures around trains. *J Journal of Wind Engineering & Industrial Aerodynamics* 2010; 98(1): 34-46.
7. IIDA, MATSUMURA T, NAKATANI K, et al. Effective nose shape for reducing tunnel sonic boom. *J Railway Technical Research Institute Quarterly Reports* 1997; 38(4):206-211
8. IIDA M, MATSUMURA T, FUKUDA T, et al. Optimization of Train Nose Shape for Reducing Impulsive Pressure Wave from Tunnel Exit. *J Nihon Kikai Gakkai Ronbunshu B Hen/transactions of*

- 
- the Japan Society of Mechanical Engineers Part B* 1996; 62(596): 1428-1435.
9. Kikuchi K, Iida M, Fukuda T. Optimization of Train Nose Shape for Reducing Micro-pressure Wave Radiated from Tunnel Exit. *J Journal of Low Frequency Noise Vibration & Active Control* 2011; 30(1):1-19.
  10. KU Y C, RHO J H, YUN S H, et al. Optimal cross-sectional area distribution of a high-speed train nose to minimize the tunnel micro-pressure wave. *J Structural & Multidisciplinary Optimization* 2010; 42(6): 965-976.
  11. Bellenoue M, Moriniere V, Kageyama T. Experimental 3D simulation of the compression wave due to train tunnel entry. *J Journal of Fluids and Structures* 2002; 16(5): 581-595.
  12. KWON H B, JANG K H, KIM Y S, et al. Nose Shape Optimization of High-speed Train for Minimization of Tunnel Sonic Boom. *J Jsme International Journal* 2001; 44(3): 890-899.
  13. LEE J, KIM J. Approximate optimization of high-speed train nose shape for reducing micropressure wave. *J Structural & Multidisciplinary Optimization* 2008; 35(1): 79-87.
  14. KU Y C, PARK H I, KWAK M H, et al. Multi-Objective Optimization of High-Speed Train Nose Shape Using the Vehicle Modelling Function; In: *proceedings of the AIAA Aerospace Sciences Meeting Including the New Horizons Forum and Aerospace Exposition, F, 2010*.
  15. ZHAO H, LI Q, LI X, et al. A design method for high-speed train nose shape under multi-line cases. *J SL: Structural Longevity* 2012; 7(2):87-103.
  16. XIONG J, LI T, ZHANG J Y. Shape optimization of high-speed trains under multi runing conditions. *J Scientia Sinica Technologica* 2016; 46:313-322.
  17. CHIU T W, SQUIRE L C. An experimental study of the flow over a train in a crosswind at large yaw angles up to 90°. *J Journal of Wind Engineering & Industrial Aerodynamics* 1992; 45(1): 47-74.
  18. KRAJNOVIĆ S. Optimization of Aerodynamic Properties of High-Speed Trains with CFD and Response Surface Models. *The Aerodynamics of Heavy Vehicles II: Trucks, Buses, and Trains* 2009; 197-211.
  19. LORRIAUX E, BOURABAA N, MONNOYER F. Aerodynamic optimization of railway motor coaches. In: *1th World congress on railway research* 2006;
  20. VYTLA V V S, HUANG P, PENMETSA R. Multi-Objective Aerodynamic Shape Optimization of High Speed Train Nose Using Adaptive Surrogate Model; In: *proceedings of the Aiaa Applied Aerodynamics Conference, F, 2010*.
  21. MUÑOZ PANIAGUA J, GARCÍA GARCÍA J, CRESPO MARTÍNEZ A. Aerodynamic Optimization of High-Speed Trains Nose using a Genetic Algorithm and Artificial Neural Network. *CFD & Optimization*, Antalya-Turkey 23 May -25 May, 2011.
  22. Suzuki M, Nakade K. Multi-objective design optimization of high-speed train nose. *J Journal of Mechanical Systems for Transportation and Logistics* 2013; 6(1): 54-64.
  23. MUÑOZ-PANIAGUA J, GARCÍA J, CRESPO A. Genetically aerodynamic optimization of the nose shape of a high-speed train entering a tunnel. *J Journal of Wind Engineering & Industrial Aerodynamics* 2014; 130:48-61.
  24. MENG-GE Y U, ZHANG J Y, ZHANG W H. Multi-objective optimization design method of the high-speed train head. *J Journal of Zhejiang Universityence A* 2013; 14(9): 631-641.
  25. MENGGE Y U, ZHANG J, ZHANG W. Multi-objective Aerodynamic Optimization Design of the Streamlined Head of High-speed Trains under Crosswinds. *J Journal of Mechanical Engineering* 2014; 50(24):122
  26. MING L I, MING-GAO L I, GUO-QING L I, et al. Optimized Design of Parameteric-driven Aerodynamic Shape of High-speed EMU Head-type. *J Tiedao Xuebao/journal of the China Railway Society* 2013; 35(11): 14-20.
  27. CUI K, WANG X P, HU S C, et al. Shape Optimization of High-Speed Train with the Speed of 500kph. *Springer Berlin Heidelberg*, 2012, p 187-197.
  28. YAO SB, GUO DL, SUN Z, et al. Optimization design for aerodynamic elements of high speed trains. *J Computers & Fluids* 2014; 95(21): 56-73.
  29. YAO S, GUO D, SUN Z, et al. Multi-objective optimization of the streamlined head of high-speed trains based on the Kriging model. *J Science China Technological Sciences* 2012; 55(12): 3495-3509.
  30. YAO S, GUO D, YANG G. Three-dimensional aerodynamic optimization design of high-speed train nose based on GA-GRNN. *J Science China Technological Sciences* 2012; 55(11): 3118-3130.
  31. Yao S B, Guo D L, Yang G W. Aerodynamic optimization of high-speed train based on RBF Mesh deformation. *J Chinese Journal of Theoretical and Applied Mechanics* 2013; 45(6): 982-986.

- 
32. YAO S, GUO D, SUN Z, et al. A modified multi-objective sorting particle swarm optimization and its application to the design of the nose shape of a high-speed train. *J Engineering Applications of Computational Fluid Mechanics* 2015; 9(1): 513-527.
  33. YAO S B, GUO D L, SUN Z X, et al. Parametric design and optimization of high speed train nose. *J Optimization & Engineering* 2016; 17: 605-630.
  34. SEDERBERG T W, PARRY S R. Free-form deformation of solid geometric models. *ACM SIGGRAPH computer graphics* 1986; 20(4): 151-160.
  35. LI R, XU P, PENG Y, et al. Multi-objective optimization of a high-speed train head based on the FFD method. *J Journal of Wind Engineering and Industrial Aerodynamics* 2016; 152:41-49.
  36. LEE C, KOO D, ZINGG D W. Comparison of B-Spline Surface and Free-Form Deformation Geometry Control for Aerodynamic Optimization. *J AIAA Journal* 2017; 55(1): 228-240.
  37. SUN Z, SONG J, AN Y. Optimization of the head shape of the CRH3 high speed train. *J Science China Technological Sciences* 2010; 53(12): 3356-3364.
  38. LAMOUSIN H J, WAGGENSPACK W N, JR. NURBS-based free-form deformations. *J IEEE Computer Graphics & Applications* 1994; 14(6): 59-65.
  39. You LH, Yang XS, Pachulski M, Zhang JJ. Boundary constrained swept surfaces for modelling and animation. *Computer Graphics Forum* 2007; 26(3): 313-322.
  40. Zhang JJ, You LH, PDE based surface representation - vase design. *Computers & Graphics* 2002; 26: 89-98.
  41. Zhang J, You L H. Fast surface modelling using a 6th order PDE. *C Computer Graphics Forum* 2004; 23(3): 311-320.
  42. Jiang C X, Liang X F. Effect of the Vehicle Aerodynamic Performance Caused by the Height and Position of Wind-Break Wall. *Zhongguo Tiedao Kexue/china Railway Science* 2006;27(2):66-70.
  43. Gao G J, Duan L L. Height of wind barrier on embankment of single railway line. *Zhongnan Daxue Xuebao* 2011; 42(1):254-259.
  44. Murata K, Nagakura K, Kitagawa T, et al. Noise Reduction Effect of Noise Barrier for Shinkansen Based on Y-shaped Structure. *Quarterly Report of Rtri* 2006; 47(3):162-168.
  45. Hothersall D C, Horoshenkov K V, Morgan P A. Scale modelling of railway noise barriers. *Journal of the Acoustical Society of America* 1998; 103(2):207-223.
  46. Chen L, Research on the technology of the parameterized facial expression animation based on FFD. *Master thesis. Hangzhou: Zhejiang University,2006.*
  47. Wu Z, Chen Z, Ding W. Digital Design of Streamlined EMU Head Car and Its Smoothness Evaluation. *International Journal of Hybrid Information Technology* 2015; 8(7): 117-132.
  48. CHEN Z, WU Z. Optimization Method of Train Surface Based on NURBS Theory. *Railway Locomotive & Car* 2014; 1: 006.
  49. DONG Y, XU Y, QIU Y. Numerical simulation of the aerodynamic behaviors of a high-speed train traveling on the bridge. *J Railway Locomotive & Car* 2008; 3: 006.
  50. Howe M S. On the compression wave generated when a high-speed train enters a tunnel with a flared portal[J]. *Journal of Fluids and Structures*, 1999, 13(4): 481-498.
  51. Mok J K, Yoo J. Numerical study on high speed train and tunnel hood interaction[J]. *Journal of wind engineering and industrial aerodynamics*, 2001, 89(1): 17-29.
  52. Lei Z, Hongqi T, Mingzhi Y. Influence on tunnel aerodynamic effects by slope of hat oblique tunnel portal. *J Journal of Central South University, Science and Technology* 2013; 44(2): 817-822.